

Computation of Surface Energies in an Electrostatic Point Charge Model:

II. Application to Zircon (ZrSiO_4)

C.F. Woensdregt

Institute of Earth Sciences, Utrecht University, Department of Geochemistry, Section of Crystallography, P.O. Box 80.021, 3508 TA Utrecht, The Netherlands

Received July 5, 1991 / Accepted January 13, 1992

Abstract. In zircon (ZrSiO_4), four different Periodic Bond Chains (PBCs) can be described, i.e. $[001]$, $\langle 100 \rangle$, $\langle 1/2 \ 1/2 \ 1/2 \rangle$ and $\langle 1/2, \ 1/2, \ 1 1/2 \rangle$. F faces which grow slowly according to a layer mechanism, are $\{100\}$ and $\{011\}$. Calculation of attachment energies, which are supposed to be directly proportional to the growth rates, is performed in electrostatic point charge models, model I: $\text{Zr}^{4+} \text{Si}^{4+} \text{O}_4^{2-}$, model II: $\text{Zr}^{4+} \text{Si}^{2+} \text{O}_4^{1.5-}$ and model III $\text{Zr}^{4+} \text{Si}^0 \text{O}_4^{1-}$. The theoretical growth form is short prismatic following $\{100\}$ and is terminated by the dipyramid $\{011\}$. The lower the oxygen charge the more elongated is the crystal parallel to the c axis. The slice d_{011} can be defined either bounded by zirconium (d_{011}^A) or by silicate tetrahedra (d_{011}^B). As these slice boundaries differ in height of one half slice with thickness d_{022} , and as these half slices d_{022}^A and d_{022}^B are F faces, the growth of $\{011\}$ may also take place by elementary growth layers of thickness d_{022} . In that case the growth rates of $\{011\}$ increase and the growth models are even more prismatic. The S form $\{031\}$ could only be present on the theoretical growth form with formal charges, provided that the growth of $\{011\}$ takes place with half slices d_{022} and the adsorption of impurities establishes additional strong bonds parallel to its slice boundaries. On the models with lower silicon and oxygen charges the form $\{031\}$ is not present, but a reduction of the attachment energy of less than 0.1 percent would result into the appearance of $\{031\}$ on these models as well. If $\text{O} - \text{H} \cdots \text{O}$ bonds could be formed by adsorption of protons, silica complexes or water molecules, additional hydrogen bonds parallel to $\langle 110 \rangle$ would establish the F character of $\{110\}$ and $\{001\}$, which has been observed sometimes on minerals and synthetic crystals. Neutrally charged solvated silica complexes, such as $\text{Si}(\text{OH})_4 \cdot 2\text{H}_2\text{O}$, present as impurities on kink sites could reduce the growth rate of the forms $\{110\}$ and $\{001\}$. $\text{NH}_4\text{H}_2\text{PO}_4$ (ADP, Biphosphammite) has a crystal structure similar to that of zircon. The F forms of ADP are also $\{100\}$ and $\{011\}$. The typical tapering observed on ADP crystals grown from Cr bearing aqueous solutions due to the presence of $\{0kl\}$ with

$k > l$ is not common for zircon. The S form $\{031\}$ of ADP has such a relatively low attachment energy that it could also be present on the theoretical growth form.

Introduction

The morphology of zircon (ZrSiO_4) has already been analysed by Hartman (1956) in relation to the crystal structure. For that purpose, the crystal structure was reduced to Zr^{4+} and SiO_4^{4-} ions, which are assumed to be the building units during the crystallization process. The silicate ion was considered to be located on the site of the silicon atom. Neither the exact position of the oxygen ions nor the slice configuration at the scale of the individual oxygen ions had been taken into account. Periodic Bond Chains (PBCs) were described parallel to $[001]$, $\langle 100 \rangle$, $\langle 1/2 \ 1/2 \ 1/2 \rangle$ and $\langle 110 \rangle$. Later Hartmann (1959) demonstrated that the $\langle 110 \rangle$ PBC has no physical meaning. Hence F faces parallel to at least two PBCs are $\{010\}$ and $\{011\}$, while $\{110\}$, $\{112\}$ are S faces.

In the present study of zircon, the complete silicate ion is taken into account and special emphasis will be given to the different slice configurations which especially exist for the slice d_{011} . Furthermore the attachment energies will be computed in electrostatic point charge models (Woensdregt 1992) in order to construct the theoretical growth forms.

In addition, the crystal growth of zircon will be compared with that of ADP ($\text{NH}_4\text{H}_2\text{PO}_4$), which is also known as biphosphammite.

PBC Analysis

Strong Bonds

The crystal structure data and fractional coordinates of the atoms published by Hazen and Finger (1979) have

Table 1. Crystal structure data of zircon (ZrSiO_4)

Zircon (ZrSiO_4) space group $I4_1/amd$ $a_0 = 0.66042$ nm, $c_0 = 0.59797$ nm			
model	qe_{Zr}^a	qe_{Si}^a	we_{O}^a
model I	+4	+4	-2
model II	+4	+2	-1.5
model III	+4	0	-1
atom	x	y	z
Zr(1)	0.0000	0.0000	0.0000
Si(1)	0.0000	0.0000	0.5000
O(1)	0.0000	0.1840	0.3201

The fractional coordinates of the oxygen O(1) have been obtained from the published values (x_{HF} , y_{HF} and z_{HF}) by Hazen and Finger (1979) according to the following equations: $x_{\text{O}(16)} = y_{\text{HF}} + 1/4$, $y_{\text{O}(16)} = x_{\text{HF}}$, $z_{\text{O}(16)} = z_{\text{HF}} - 1/8$. The Zr and Si atoms are numbered with $n=1, \dots, 4$: (1) x, y, z (2) $x, y+1/2, z+1/4$ (3) $x+1/2, y+1/2, z+1/2$ (4) $x+1/2, y, z+3/4$. The O atoms are numbered with $n=1, \dots, 8$: (1) x, y, z (2) $x, 1-y, z$ (3) $y, x, 1-z$ (4) $1-y, x, 1-z$ (5) $x, y+1/2, 1/4-z$ (6) $x, 1/2-y, 1/4-z$ (7) $y, x+1/2, z+1/4$ (8) $1-y, x+1/2, 1/4+z$. The coordinates of the O atoms numbered from 9 till 16 included are obtained from the symmetrical equivalent oxygens numbered from 1 to 8 included, by adding the I translation $[1/2, 1/2, 1/2]$

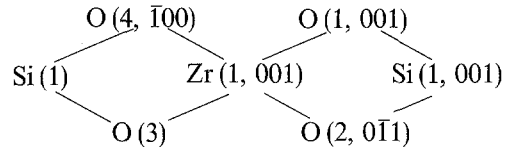
^a units in $|e|$

been used in the present study. These data are listed in Table 1, in which the numbering of the atoms has been explained as well. The zircon crystal structure (space group $I4_1/amd$) is characterised by the silicon-oxygen tetrahedra which are bonded to six different zirconium ions. On the other hand each zirconium ion is surrounded by six silicate tetrahedra, two of which by

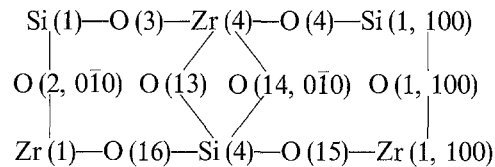
a pair of relatively long Zr–O bonds (0.2267 nm) and four others only by one shorter Zr–O bond (0.2128 nm).

[001] Zone

In the projection \parallel [001] of the zircon crystal structure (Fig. 1) the [001] PBC can easily be recognised:



Within the slice d_{020} this PBC is linked to the equivalent PBC centered on Si(4) by another PBC parallel to [100]:



Being parallel to two PBCs the form $\{020\}$ is an F form. Within the slice d_{220} the [100] PBCs are not linked neither parallel to [110] nor to $\langle 1/2, 1/2, 1/2 \rangle$. So $\{110\}$ is an S face.

[100] Zone

The [100] projection (Fig. 2) shows the [100] PBCs bonded by both the already known [001] PBC and the

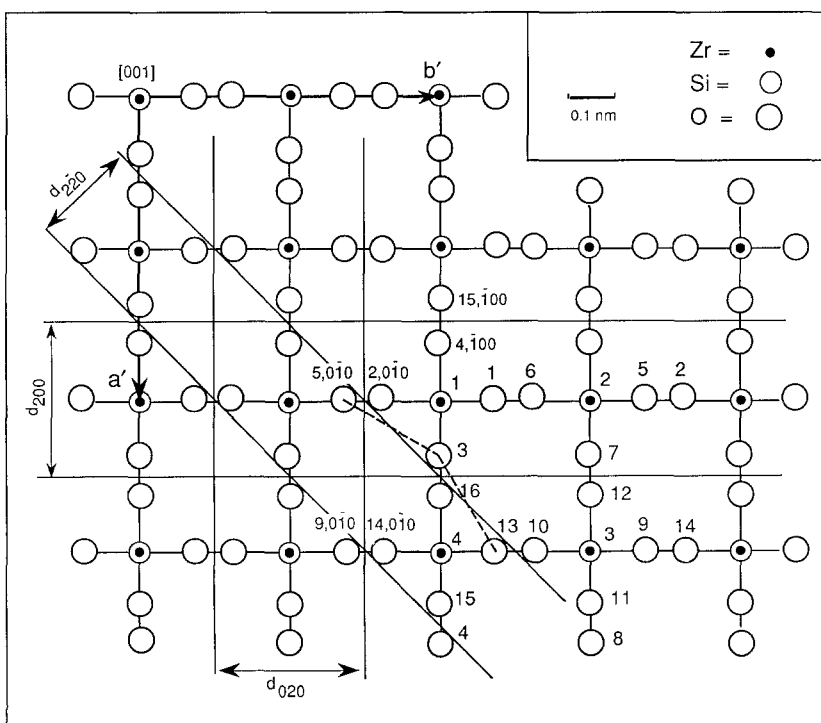


Fig. 1. Projection of the zircon crystal structure along the c -axis. The relatively short O–O distances of 0.2840 nm are given as dashed lines for O(3)

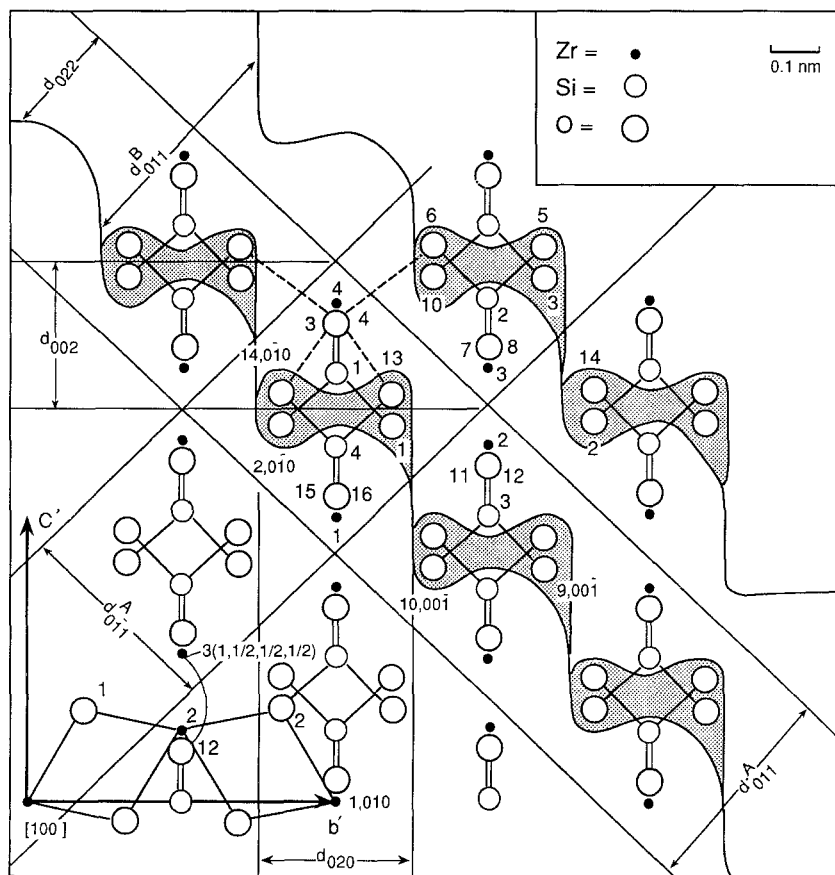


Fig. 2. Projection of the zircon crystal structure along the a -axis. Only the Si–O strong bonds have been drawn. In the left low corner the Zr–(OH,F)–Zr PBCs parallel to $[010]$ and $[\frac{1}{2} \frac{1}{2} \frac{1}{2}]$ are drawn. For O(3) the four equivalent short O–O bonds are drawn as dashed lines

$\langle \frac{1}{2} \frac{1}{2} \frac{1}{2} \rangle$ PBC

O(1)

Si(1)–O(3)–Zr(4)–O(10)–Si(3, 001)

O(4, $\bar{1}00$) (\equiv Si(1, $\frac{1}{2} \frac{1}{2} \frac{1}{2}$))

resulting in the F character of $\{020\}$ and $\{011\}$. The slice d_{011} can be defined either as slice d_{011}^A bounded by Zr ions or as slice d_{011}^B bounded by oxygen ions of the silicate tetrahedra. The slice d_{011}^B is not only undulated in the plane of projection, but also in the third dimension, if silicon-oxygen bonds should not be broken by the slice boundaries. The shaded area of Fig. 2, between the silicon atoms Si(1) and Si(4), contains two boundaries, one with Si(1) linked to O(1) and O(2,0 $\bar{1}0$) which are all situated at height 0, and the other with Si(4) bonded to O(13) and O(14,0 $\bar{1}0$), all at height 0.5.

Just as in case of ADP (Aguiló and Woensdregt 1984) all forms $\{0kl\}$ with $k > l$ are S forms. For the face (001) the slice thickness must comply with the conditions for $\{00l\}$: $l = 4n$. Within a slice of this thickness the $[100]$ PBC does not exist and so $\{004\}$ is a K face.

$\langle \frac{1}{2} \frac{1}{2} \frac{1}{2} \rangle$ zone

The I cell symmetry of zircon results in halving the period of the PBC parallel to $[111]$. The $\langle \frac{1}{2} \frac{1}{2} \frac{1}{2} \rangle$ transla-

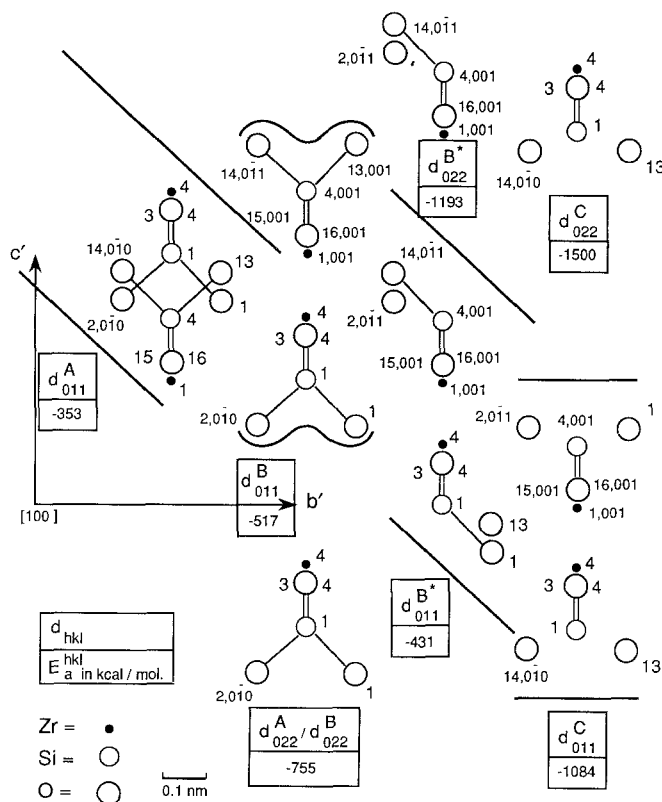


Fig. 3. Several possibilities for the slice configuration of d_{011} as seen in the projection parallel to the a -axis. In the boxes below each configuration the slice identifier with its attachment energy is indicated

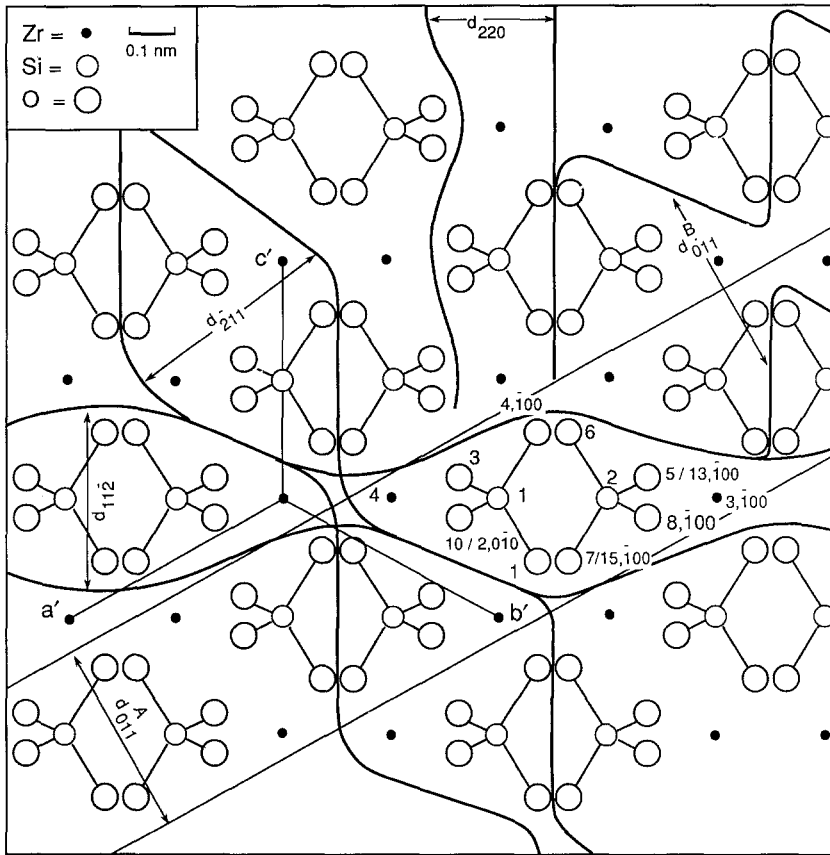


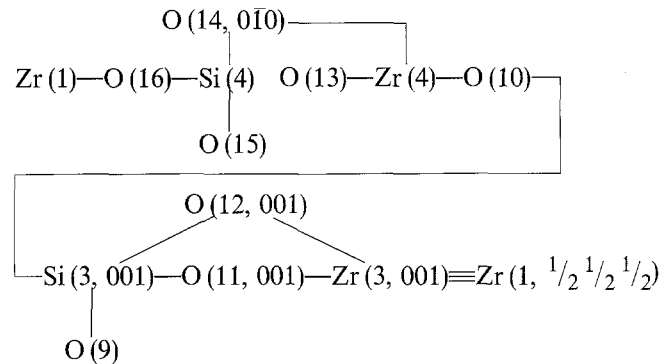
Fig. 4. Projection of the zircon crystal structure along $[1/2 \ 1/2 \ 1/2]$

tion period is the shortest translation period (0.5545 nm) of all PBCs. The $\langle 1/2 \ 1/2 \ 1/2 \rangle$ PBC described in the previous section is in the $\langle 1/2 \ 1/2 \ 1/2 \rangle$ projection (Fig. 4) a partial PBC, which means that the PBC is stoichiometric but has a dipole moment perpendicular to its vector. It can be transformed into a complete PBC by taking it together with its equivalent one centered around Si(2) and Zr(3, $\bar{1}00$).

The $[1/2 \ 1/2 \ 1/2]$ projection contains besides the already described F form $\{011\}$, the forms $\{112\}$, $\{211\}$ and $\{110\}$. The d_{011}^A delineated in Fig. 4 is identical to the d_{011}^A defined with the $[100]$ PBC (Fig. 2), just as the alternative slice d_{011}^B . The $\{112\}$ and $\{121\}$ are S forms as their slices are only parallel to the $\langle 1/2 \ 1/2 \ 1/2 \rangle$ PBC and other strong bonds parallel to their slice boundaries are absent. Moreover $\{110\}$ is in this projection a K face as the complete $\langle 1/2 \ 1/2 \ 1/2 \rangle$ PBC does not fit within the slice boundaries of d_{220} .

$$\langle 1/2, 1/2, 1/2 \rangle$$

The fourth PBC parallel to $\langle 1/2, 1/2, 1/2 \rangle$ will not change the already described character of the crystal forms of zircon. The configuration of this PBC (see also Fig. 1) is as follows:



Qualitative Results

Four complete PBCs are present in zircon, parallel to $\langle 100 \rangle$, $[001]$, $\langle 1/2 \ 1/2 \ 1/2 \rangle$ and $\langle 1/2, 1/2, 1/2 \rangle$. The qualitative PBC analysis of ADP (Aguiló and Woensdregt 1984) leads to identical results. Consequently the only F forms of both, zircon and ADP, are $\{011\}$ and $\{100\}$. The stereographic projection, given in Fig. 5, shows the PBCs and the classification of the most prominent crystal forms.

The surface of the slice of d_{020} is occupied by oxygen atoms, while that of $\{011\}$ is bounded either by positive

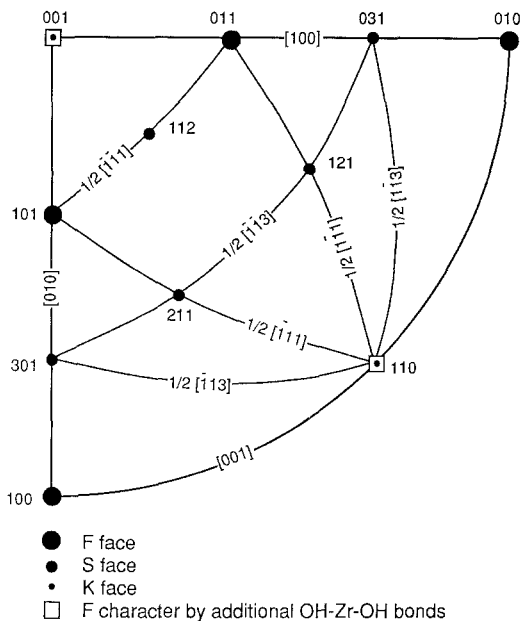


Fig. 5. Stereographic projection of zircon in which the PBCs and the classification of the most prominent crystal forms are indicated

zirconium ions (d_{011}^A) or negative silicate ions (d_{011}^B). The role of impurities and the surface diffusion will be different for each of these slice configurations.

Attachment Energies

Models

Having classified the crystal forms in F, K and S forms, the quantitative morphological importance must be established. Hartman and Bennema (1980) indicated that the growth rate of F faces is directly proportional to their attachment energies. The calculations which can be performed in the electrostatic point charge models have been described in the foregoing paper (Woensdregt 1992). By applying the Madelung formula for the potential induced by an infinite row of equally spaced point charges, it is possible to calculate the slice energy, E_s , the attachment energy, E_a and the crystal energy, E_c . The exact definitions of these energies are given by Woensdregt (1992). The following relation is valid:

$$E_c = E_s + E_a \quad (1)$$

Three different point charge models have been used for the calculation of these types of energy. The first model (I) with the formal charge is $Zr^{4+}[Si^{4+}O_4^{2-}]$, and the two other models with the reduced silicon and oxygen charges are: $Zr^{4+}[Si^{2+}O_4^{-1.5}]$ (model II) and $Zr^{4+}[Si^0O_4^{-1}]$ (model III). As the ionicity of the Si–O bond is lower than 100%, this reduction of the formal charges may be considered as a measure of the influence of the covalency on the growth rates.

Table 2. Chain energies in kJ/mol

[100]/ d_{hkl}		
hkl	E_{ch}	E_{ch}/E_s
011 ^A	–25613	0.97
011 ^B	–24761	0.96
022 ^A	–23870	0.97
011 ^{B*}	–23596	0.91
022 ^{B*}	–22763	0.93
011 ^C	–22535	0.97
022 ^C	–21865	1.01
020	–25655	0.96
031	–25655	1.00
[$1/2 \ 1/2 \ 1/2$]/ d_{hkl}		
112	–22579	1.02

Chain Energies

There are four different PBCs in the zircon structure. The chain energy is a function of the chain configuration which is not always the same, even for the same direction. This configuration is also determined by the slice thickness d_{hkl} in which the chain is situated. Therefore the chain energies are given for a particular PBC [UVW] situated in one specific slice d_{hkl} ([UVW]: d_{hkl}) and listed in Table 2.

The [100]/ d_{011}^A has the highest energy (–25612 kJ/mol) compared to that of [100]/ d_{011}^B (–24761 kJ/mol). All other PBCs, e.g. [100]/ d_{011}^{B*} and [100]/ d_{011}^C , have much lower energy values. Halving the slice thickness reduces the chain energy as well. In addition, the chain energy contribution to the total slice energy is listed in Table 2. In all cases this contribution is more than 90 percent.

Another interesting aspect is that sometimes the chain energy is more negative than the total slice energy. In that case, the contributions of all the other chains except the central PBC are positive. This means that, within the slice, a repulsive force exists between the central PBC and the other chains. The most important examples of such chains are [$1/2 \ 1/2 \ 1/2$]/ d_{112} and [100]/ d_{031} . For the latter one, the difference between the chain energy E_{ch}^{031} and the slice energy E_s^{031} is only 19 kJ/mol. Although the chain energy could be a measure of the strength of a PBC, it varies so much with its configuration, that a qualitative classification of the PBCs based on E_{ch} is not very useful.

Slice Energies and Attachment Energies

Once the energy of slice (hkl), $E_s^{(hkl)}$, and the crystal energy, E_c , of a certain compound are known, the attachment energy, $E_a^{(hkl)}$ of that particular slice need not to be computed as these energies are related by (1). Only if the slice is polar, the attachment energy cannot be computed

Table 3. Chain energy, E_{ch} , slice energy, E_s , partial attachment energies, E_m , and attachment energy, E_a of slice d_{011}^A , in kJ/mol

ion	E_{ch}	E_s	E_1	E_2	E_3	E_a
Zr	-6281	-7312	-1381	12	-1	-1370
Si	-9753	-10162	167	-2	-1	164
O	-9579	-8909	-277	3	1	-273
Total	-25613	-26383	-1491	13	-1	-1479

and must be calculated by subtracting the slice energy from the crystal energy. This has been performed for all the polar slices d_{022} , which will be discussed hereafter. Although in all other cases it is not necessary to calculate both, the attachment energy and the slice energy, they are computed almost always. The constant sum of slice energy and attachment energy enables one to check that no significant contributions have been neglected either in case of the slice energy by calculating the contributions of PBCs at distances of several nm through a power series or in case of the attachment energy by not taking into account the contributions of the partial attachment energies of the slices E_{m+1} , E_{m+2} , etc., when the calculated value of E_m is less than a minimum value. This minimum is normally chosen in the order of a few hundreds of kJ/mol (for further details see Woensdregt 1992). An example of such a calculation is given in in Table 3, which summarizes the partial energies for the calculation of the slice energy E_s^{011A} and the attachment energy E_a^{011A} based on the [100] PBC. The attachment energy converges very rapidly, the third slice contributes only -1 kJ/mol to the attachment energy, and therefore, the contributions of all layers with slice number $m > 3$ can be neglected. The effective contributions to the attachment energy are confined to the interaction energies of the growth unit attached to the crystal surface with the underneath part of the crystal which is only about 1.3 nm thick, i.e. three slices d_{011} . There are rather significant differences among the contributions to the attachment energy with respect to the ion type. The largest contribution to the energy E_a^{011A} is made by the zircon ions. To the total amount of attachment energies contributed by the zircon ions (-1369 kJ/mol) the Zr(4) ion alone contributes -1336 kJ/mol. For the purpose of calculation, the crystal was divided into slices d_{011} which formed the half crystal by a translation along the positive c axis (for further details see Woensdregt 1992). As the growth of the crystal proceeds with the formation of new slices d_{011} , the Zr(4) ion is the closest Zr ion to the surface of the growing crystal (Fig. 2). Hence the partial attachment energy of Zr(4) is much higher than that of Zr(1). The contribution of Zr(4) is also the highest compared with those of all other ions, which means that on a flat surface of (011)^A the probability to be attached as the first ion on such a surface is the highest for Zr(4). From that moment on, the surface configuration is changed, and no further order of attachment can be derived from the calculated partial attachment energies.

Table 4. Slice and attachment energies of zircon in kJ/mol

model I: $Zr^{4+}Si^4+O_4^{2-}$			
d_{hkl}	E_s 1)	E_a	E_c^a
020	-26587	-1275	-27862
011 ^A	-26383	-1479	-27862
011 ^B	-25698	-2165	-27863
022 ^A	-24701	-3161 ^b	-27862
011 ^{B*}	-26057	-1803	-27860
022 ^{B*}	-24498	-4997 ^b	-27862
011 ^C	-23321	-4539	-27861
022 ^C	-21581	-6281 ^b	-27862
031	-25636	-2225	-27861
112	-22140	-5720	-27861
model II: $Zr^{4+}Si^{2+}O_4^{1.5-}$			
020	-14687	-1163	-15850
011 ^A	-14363	-1487	-15850
011 ^B	-13789	-2061	-15851
022 ^A	-12743	-3106 ^c	-15850
031	-13661	-2189	-15849
model III: $Zr^{4+}Si^0O_4^{1-}$			
020	-8002	-990	-8992
011 ^A	-7534	-1457	-8992
011 ^B	-7113	-1880	-8993
022 ^A	-6048	-2945 ^d	-8993
031	-6908	-2083	-8992

^a not corrected for the Coulomb interactions within the $[SiO_4]^{4-}$ ion

^b calculated $E_a = E_c - E_s = -27862 - E_s$

^c calculated $E_a = E_c - E_s = -15850 - E_s$

^d calculated $E_a = E_c - E_s = -8993 - E_s$

Theoretical Growth Forms

In the so-called Wulff plot (Wulff 1901), the distance from the central point to a certain face (hkl) is taken directly proportional to the absolute value of the attachment energy of that face. The innermost closed surface of the three-dimensional Wulff plot represents the theoretical growth form. This growth form is constructed only on the basis of the attachment energy data calculated in an electrostatic point charge model, and is, therefore, as reliable as the model represents the reality. Hence, the theoretical growth form shows the influences of the crystal structure on the growth rates, not taking into account the action of impurities, the environmental symmetry, the Born repulsion, and other than electrostatic interaction energies. However, by lowering the formal charges the influence of the covalency can be estimated. All theoretical growth forms presented in this paper have been obtained by using the computer programs CRYSTALFORM and CRYSTALDRAW (Strom 1979).

The calculated slice, attachment and crystal energies are listed in Table 4. The slice and crystal energies are not corrected for the Coulomb interactions within the $[SiO_4]^{4-}$ ion, which is assumed to be one of the crystallizing units. The corrections are for both the crystal and slice energy in case of model I ($Zr^{4+}Si^4+O_4^{2-}$):

–12983 kJ/mol, and for model II ($\text{Zr}^{4+}\text{Si}^{2+}\text{O}_4^{1.5-}$): –2166 kJ/mol, and for model III ($\text{Zr}^{4+}\text{Si}^0\text{O}_4^{1-}$): +3603 kJ/mol. The corrected crystal energies are –14879, –13683 and –12596 kJ/mol for model I, II and III, respectively. Only the values of the prism {100} and the dipyramids {011} and {031} are given for all the models. The attachment energies of all the other slices are too high to be present on the theoretical growth form. The attachment energy of (112) in model I (–5720 kJ/mol) is an example of these high values for an S face. The slice d_{020} has in all the models the lowest attachment energy. This does not mean that all growth forms have a distinct prismatic habit, as the {011} attachment energies can have much higher values and still be present as a dominant form (model Ia, Fig. 6). Such an effect is caused by the geometrical factor (Woensdregt 1982), which is purely the geometrical relation of one crystal form to its other neighbours. In Fig. 6 the theoretical growth forms are shown for all models.

The Dipyramid {011}. The slice d_{011} cannot be drawn unambiguously. The slice configuration with the lowest attachment energy (e.g., model I: –1479 kJ/mol), called slice d_{011}^A , is shown in Fig. 1. In that case the slice is bounded by Zr ions. The growth models Ia, IIa and IIIa are based on these slice configurations. It is also possible to trace the slice bounded by silicate ions, the slice d_{011}^B configuration (see also Fig. 1). Both configurations and all the other ones based on half slices d_{022} , which will be discussed later are summarized in the [100] projection of Fig. 3. The attachment energy of d_{011}^B is much higher (–2165 kJ/mol) than that of slice d_{011}^A . If more than one slice configuration can be drawn, which differ from each other in height by submultiples of d_{hkl} , the growth may also take place by elementary growth layers with a thickness of a submultiple of d_{hkl} as postulated by Hartman and Heijnen (1983) and Heijnen (1986). In that case the half slice must be an F face as well, which is true for both slices, d_{022}^A and d_{022}^B . The half slices d_{022}^A and d_{022}^B are symmetrically equivalent by the presence of a 2_1 screw axis and have the same attachment energy (–3161 kJ/mol).

It is also possible to delimit the boundaries of d_{011}^B as straight as those of d_{011}^A . These new configurations, d_{011}^{B*} and d_{011}^C have also their own half slices, respectively d_{022}^{B*} and d_{022}^C (see also Fig. 3). The slice configurations d_{011}^{B*} and d_{011}^C are not very probable as they are based on the formation of Si–O bonds during the crystallization. Only if the silicate growth units do not consist of $[\text{SiO}_4]^{4-}$ ions, such slice configurations should be considered as alternatives. The attachment energies of both half slices are more negative than those of all other half slices as Si–O bonds are broken by the slice boundaries. Since the slice energy of any stoichiometric set of Zr, Si and O ions can be computed, the results must be carefully examined. An unrealistic choice of the growth unit with one or more broken Si–O bonds per molecule leads to attachment energies, which are more negative than that of the energetically most favourable F slice configuration. Hence other slice configurations for the half slice than d_{022}^A are not very likely to have

an influence on the growth of the face (011). In Table 4 all the computed energies for all half slices of all models are listed.

The surface energy of (011)^A can be computed from the known $E_{m\ 011^A}$ energies, where $m=1, 2, 3$, etc., (Woensdregt 1992).

The surface energy for (011)^A amounts to 8277 mJm^{–2} and is defined as all other surface energies calculated in the electrostatic point charge models with reference to vacuum. The corresponding surface energy with reference to the actual growth medium could be in the order of one hundred mJm^{–2}, which is a reasonable value for a slightly soluble salt (Söhnel 1982). For that reason, the surface energies with respect to the actual growth medium γ'_{hkl} can be estimated from the corresponding values with respect to vacuum (γ_{hkl}) as follows

$$\gamma'_{hkl} \approx 10^{-2} \gamma_{hkl}. \quad (2)$$

The same correction factor holds also for the surface energy per mole $E'_{s(i)}$ with respect to the actual growth medium, that will be computed from the surface energy per mole with respect to vacuum, $E_{s(i)}$, as follows:

$$E'_{s(i)} = 10^{-2} E_{s(i)} \quad (3)$$

According to Heijnen (1986) the relative area, x_i , occupied by the N different F configurations of {hkl} depends on the surface energy per mole with reference to the growth medium via a Boltzmann type of distribution

$$x_i = \frac{\exp\left[\frac{E'_{s(i)}}{RT}\right]}{\sum_{i=1}^N \exp\left[\frac{E'_{s(i)}}{RT}\right]} \quad (4)$$

where RT is equal to 7.25 kJ/mol at 600° C, to 10.6 kJ/mol at 1000° C, and to 12.7 kJ/mol RT at 1250° C.

The surface energies per mole for d_{011}^A ($E_{s(i)}^{011A}$) and d_{011}^B ($E_{s(i)}^{011B}$) are, respectively 1467 and 2073 kJ/mol. Following (3) and (4), the corresponding areas of (011)^A and (011)^B are, respectively 70 and 30% at 600° C, 64 and 36% at 1000° C and 62 and 38% at 1250° C. At all possible crystallization temperatures of zircon, the total area of (011)^B present is sufficiently large enough that the growth of (011) can also take place with half slices of thickness d_{022} . As this half slice has a higher negative attachment energy, the growth rate of (011) will increase and, consequently, the growth form will change. The growth rate of (011) will be proportional to $E_a^{(011)}$ at the minimum and to $E_a^{(022)}$ at the maximum. In the submodels *a (where *a=I, II or III) the attachment energies of d_{011}^A have been plotted against those of d_{020} , while in the submodels *b the attachment energies of d_{022}^A are used instead of those of d_{011} .

The dipyramid {031}. The form {031} is an S face. For ADP it has, however, such a low attachment energy that it could be present on the growth form (Aguiló and Woensdregt 1987). In that case the {031} must obtain an F character through the adsorption of impurities on the slice surface, which should provide additional strong bonds parallel to its slice boundaries.

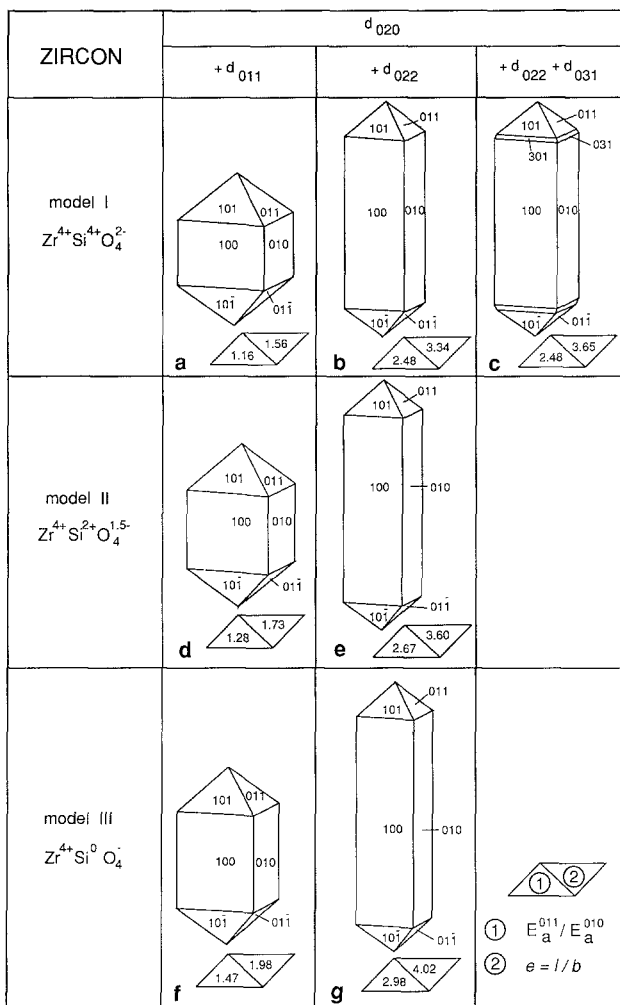


Fig. 6. Theoretical growth forms of zircon

The $\{031\}$ of zircon is not present in those models derived from the attachment energies E_a^{011} . The theoretical growth forms calculated with E_a^{022} show the form $\{031\}$ only, when the oxygen charge is equal to $-2|e|$ (model Ic). In the model IIb, with qe_o equal to $-1.5|e|$, the E_a^{031} is just too high (0.1 kJ/mol) for $\{031\}$ to be present, and in the model IIIb, with qe_o equal to $-|e|$, this difference increases to 1 kJ/mol. These limiting values, which control the presence of the $\{031\}$ on the growth form, are obtained from the CRYSTALFORM program (Strom 1979).

Quantitative Crystal Morphology

Figure 6 shows very clearly the influence of the different parameters in the point charge model calculations on the theoretical growth forms. The influence of the different slice configurations are shown horizontally, and that of the different charge distributions vertically. By lowering the charges of silicon and oxygen the habit becomes more prismatic following $\{100\}$. This effect is even more enhanced, when the attachment energies E_a^{022} instead of E_a^{011} are used. The S form $\{031\}$ could be present

on model Ib, which is presented as the separate Ic theoretical growth model.

Discussion

Natural Zircon Morphology

The relative morphological importance of the crystal forms of minerals can be estimated from their P - and F -values, respectively the *Kombinationspersistenz* and the *Fundortpersistenz* (Niggli 1923). The crystal forms of the mineral zircon with the highest P - and F -values, calculated by Hartman (1956) from an inspection of the figures published by Goldschmidt (1923), are in order of decreasing P -values as follows: $\{011\}$, $\{100\}$, $\{110\}$, $\{211\}$, $\{031\}$, $\{112\}$, etc. The first two are F faces, and the other ones S faces.

Natural zircons show a prismatic habit mostly following $\{100\}$ and terminated by $\{011\}$ dipyrramids. Sometimes they are, however prismatic following $\{110\}$ with $\{011\}$ dipyrramids (hyacinth habit, Hintze 1915, p 1628). In very rare occasions natural zircon shows the dipyrmidal habit following $\{011\}$ (Azorite habit, according to the description by Hintze 1915, p 1658). It is not easy to relate the hyacinth habit with a special rock type with a characteristic chemistry or crystallization history. Pupin et al. (1978) observed that the late overgrowths of hydrozircon rich in radioactive elements are prismatic following $\{110\}$ instead of $\{100\}$. This habit change could be related with the action of water as has been postulated by Pupin et al. (1978). The azorite habit, however, has been specially observed in peralkaline rocks (see for a review Floor 1966, p 48). Other dipyrmidal forms $\{0kl\}$ with $k>l$ are known, $\{031\}$ occurs more frequently than $\{051\}$. Additional forms such as $\{112\}$, $\{121\}$, may be present as well on natural growth forms. Cesbron et al. (1985) observed, that in the sodium-rich pyroxene syenites of Meponda (Mozambique) tabular crystals of zircon with dominant $\{001\}$ are present.

Other occurrences of tabular crystals have been reported by these authors, but always in alkaline magmatic rocks which are both saturated or supersaturated in SiO_2 (syenites and granites) and hyperalkaline (Na). Characteristic minerals in these rocks are sodic amphiboles and pyroxenes. Kostov (1973) stated that excess of SiO_2 lead to crystals, which are shorter parallel to $[001]$.

Pupin and Turco (1981) summarized the results of the typomorphological study of zircon populations in a schematic diagram, in which each type of morphology is characterized by two coordinates, the prismatic index T and the pyramidal index A . They observed that the morphology depends on temperature, chemistry and the available water content. The deviations from the theoretical morphology as derived in the present paper, which correspond with rather high A and T indices, must be due to external factors, such as impurities and supersaturation. The explanation of Pupin and Turco (1981) in terms of chemistry and water content could be seen as the influence of impurities on the crystal growth, while

the influence of the temperature must be related with the supersaturation.

The length/width ratio, also known as the elongation ratio e , which is very often used in order to describe the crystal morphology of zircon in igneous and metamorphic rocks can also be computed for the different theoretical growth models. They are 1.56, 1.73 and 1.98, respectively for model Ia, Ib and Ic, and 3.34, 3.60 and 4.02, respectively for model IIb, IIIb and IIIb. If the elongation ratio is significantly higher than four, the conclusion can be drawn, that such needle shaped crystals are due to external conditions, such as a high degree of supersaturation.

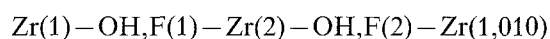
Crystal Growth Experiments

The morphology of synthetic zircon crystals grown under hydrothermal conditions from different types of solutions has been studied by Caruba (1978). The crystals have a distinct prismatic habit, if they grow in solutions in the presence of alkaline components, such as LiCO_3 , LiMoO_4 and K_2CO_3 . However, crystals grown from acid solutions are mainly dipyrmidal following $\{011\}$, and show in addition $\{001\}$. If K or Na has been added to these acid solutions as an impurity, the crystals show again prismatic forms.

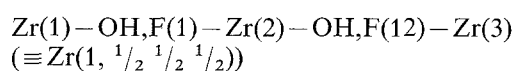
Caruba et al. (1988) described the crystal growth of zircon when using natural zircons as seeds in a sulphatic hydrothermal solution. They observed that the crystallization on $\{011\}$ is very slow with respect to that on $\{100\}$. As a result the experimental growth form shows a dipyrmidal habit following $\{011\}$, even when the seed material was prismatic.

The Role of Hydrogen Bonds in Zircon

Caruba (1978) and Caruba et al. (1988) explained such habit changes as described in the previous section by the replacement of SiO_4 tetrahedra by F_4 and $(\text{OH})_4$ ones. The presence of OH has been proven by means of infrared (IR) analysis (Caruba et al. 1985). The substitution of SiO_4 by $(\text{OH})_4$ or F_4 would lead to the destruction of the $\text{Zr}-\text{Si}-\text{Zr}$ PBCs and to the creation of $\text{Zr}-\text{OH}-\text{Zr}$ or $\text{Zr}-\text{F}-\text{Zr}$ PBCs. If in such a structure of $(\text{OH})_4$ or F_4 tetrahedra the coordination of Zr has not changed significantly, two $\text{Zr}-(\text{OH},\text{F})-\text{Zr}$ PBCs could be formed (see also the lower left corner of Fig. 2), one parallel to $\langle 010 \rangle$:



and another one parallel to $\langle 1/2 \ 1/2 \ 1/2 \rangle$:



Our model III calculation with $qe_{\text{Si}}=0$, is a model of such a structure, as the $\text{Si}-\text{O}$ bonds do not contribute to the Coulomb surface energies as computed in this model. In this model IIIa the ratio between E_a^{011}/E_a^{010} increases slightly and the theoretical growth form be-

comes even more prismatic. This is also true for the model IIIb calculations.

The second explanation of Caruba et al. (1988) is that the growth of $\{011\}$ will be reduced by the adsorption of protons on the silicate bounded surface of (011) at conditions of low pH. Thus, the differences between the surface energy of $(011)^A$ and $(011)^B$ increase as the pH decreases during the growth. The higher the adsorption the lower the probability that $\{011\}$ will be bounded by two different slices which differ just a half slice d_{022} in height. In that case the growth rate of $\{011\}$ will decrease during the growth, which leads to a more dipyrmidal habit.

As the computed values of the attachment energies are now known, the following critical remarks can be made. Adsorption of the protons will lower the surface energy in such a manner that the attachment energy of d_{011}^B will be less negative. The adsorption must have such an effect that finally the attachment energy of d_{011}^B will be much more less negative than that of d_{011}^A . Only then the growth proceeds with a slice thickness of d_{011} . The adsorption of hydrogens can be translated into a point charge model with lowered oxygen charges. The model III (with $qe_o = -|e|$) calculations indicate the extent of the adsorption effect. This model shows a reduction of the attachment energy of d_{011}^B (-1880 kJ/mol), but not to a value below that of d_{011}^A (-1457 kJ/mol). However, in this model III the qe_{Si} equals zero, which influences these calculations as well.

The presence of OH ions could, however, lead to a different interesting aspect. In the zircon crystal structure, there are four equivalent O—O distances of 0.2840 nm, which are short enough to comply with the conditions for a hydrogen bond O—H \cdots O. In the $\{001\}$ projection (Fig. 1) these short O—O bonds are drawn for the oxygen O(3). They could provide the additional strong bonds parallel to $\langle 110 \rangle$ in order to establish the F character of $\{110\}$ and to reduce its attachment energy. The same type of bonds could also change the character of $\{001\}$. All four equivalent short O—O bonds are drawn in the $[100]$ projection (Fig. 2) for the oxygen O(3). Hydrogen bonds are much weaker than ionic bonds. So the F character of $\{110\}$ and of $\{001\}$ is not so pronounced as the genuine F forms $\{100\}$ and $\{011\}$.

What are the possible sources for such additional hydrogen bonds? Caruba et al. (1985) could experimentally determine that the oxygens are partly replaced by OH in the crystal structure of zircon. The adsorption of protons on the surface of the crystal during the growth from hydrothermal solutions could lead to the replacement of oxygens by hydroxyls. The appearance of $\{001\}$ as a distinct form on the dipyrmidal crystals could be caused by the formation of additional strong $\text{Zr}-\text{OH}-\text{Zr}$ bonds.

Another conclusion may be drawn from the study of the solubility of quartz in supercritical $\text{H}_2\text{O}-\text{CO}_2$ and $\text{H}_2\text{O}-\text{Ar}$ systems by Walther and Orville (1983). Following these authors $\text{Si}(\text{OH})_4 \cdot 2\text{H}_2\text{O}$ is the dominant aqueous silica species in the supercritical regions of these systems. This silica complex consists of four hydroxyls

tetrahedrally coordinated to the silicon atom with two water molecules attached by hydrogen bonding. Their internal Si—OH and O—H...O bonds coincide with the bonding scheme of zircon. The presence of these uncharged solvated silica species could act as impurities during the growth. Once incorporated in a kink site they reduce the growth rate of the slices d_{110} and d_{001} as they are neutrally charged. In fact they poison the suitable kink positions which especially exist on {001} and {110} as has been shown before.

Instead of silica complexes also water molecules could be adsorbed on the surface. In that case the hydrogen bonds of the water molecule act in the same way as those of the silica complex.

ADP

ADP ($NH_4H_2PO_4$ or biphosphammite) has a crystal structure which is rather similar to that of zircon. The most important differences are, the lack of centrosymmetry in case of ADP (space group $I\bar{4}2d$) and the presence of two hydrogens per molecule. In supersaturated solutions of which the pH is about 4, the ADP is almost completely dissociated into $[NH_4]^+$ and $[H_2PO_4]^-$ ions (Sillen 1959). The only bonds to be taken into consideration as strong bonds (Aguiló and Woensdregt 1984) are the $N-H_N...O$ bonds between the crystallization units $[NH_4]^+$ and $[H_2PO_4]^-$. Each $[H_2PO_4]^-$ ion is bonded to six neighbouring ammonium ions by strong bonds. These bonds can be divided in two bonds with the relative large $N-H_N...O$ distance of 0.3170 nm, and four ones with the shorter $N-H_N...O$ distance of 0.2909 nm. Each phosphate tetrahedral group is bonded to four others by the hydrogen atoms, H_O , forming the hydrogen bond $O-H_O...O$. This hydrogen bond is not to be considered as a strong bond, because the hydrogen bond involved is too weak to overcome the ionic repulsion between the two negatively charged $[H_2PO_4]^-$ ions.

Zircon and ADP are partly different with respect to the character of their strong bonds. Although their bonding scheme is almost identical, their charge distributions are quite distinct, due to the presence of ammonium instead of the zirconium ions, the hydrogens and the phosphate ions with the central P^{5+} ion instead of the silicate ion with the central Si^{4+} . This could imply for zircon a significant deviation from the theoretical growth forms which have already been computed for ADP (Aguiló and Woensdregt 1987).

ADP and zircon theoretical growth forms differ from each other by the fact that those ADP models based on the d_{011} dipyramidal growth are almost always dipyramidal. Only if the growth of {011} proceeds with slices of thickness d_{022} the ADP growth forms are prismatic. For zircon the E_a^{011}/E_a^{010} ratio is 1.16, 1.28, 1.47, respectively for the models Ia, Ib and Ic. The corresponding values of the ADP models with for both types of hydrogen a qe_H equal to half the formal one, are 0.55, 0.66 and 0.88 (Aguiló and Woensdregt 1987). Only the last ADP model has the form {010}. ADP crystals grown from an Cr bearing aqueous solution show very often

the so-called tapering, which is caused by the presence of the S forms {0kl} with $k > l$, in addition to the form {011}. The S form {031} of ADP has such a low attachment energy that it could be present on the theoretical growth forms. However two conditions must be fulfilled. First the growth rate of {031} must be directly proportional to its growth rate, so it must grow as an F face. The presence of impurities must implicate the formation of strong bonds parallel to the slice boundaries of {031} in order to establish the characteristics of an F face, i.e. being parallel to two different sets of PBCs. Secondly the growth of {011} must take place via half slices (Aguiló and Woensdregt 1987). Tapering of zircon crystals is not very common, which is confirmed by the calculations of the attachment energies. Only if $qe_o = -2|e|$ the {031} is present (model Ibc). In all other models {031} is absent, although only a slight reduction of the attachment energies would lead to the appearance of {031} on the other *.b models. It seems that the hydrogens located in ADP at the boundaries of the slice d_{031} , just situated in between two adjacent PBCs, must reduce the attachment energy just enough in order that {031} could be present on so many growth forms. This is also corroborated by the fact that on the computed growth models the morphological importance is directly proportional with the qe_H . In models with a low qe_H the {031} is absent or strongly reduced, see also Fig. 3c in the paper by Aguiló and Woensdregt (1987).

Conclusions

- 1) In zircon the PBCs are parallel to $\langle 100 \rangle$, $\langle 1/2 \ 1/2 \ 1/2 \rangle$, $\langle 001 \rangle$ and $\langle 1/2, 1/2, 1 1/2 \rangle$. The only F forms are the prism {100} and the dipyramid {011}.
- 2) The surface of the prism {100} consists of the oxygens belonging to the silicate ions. The boundary of {011} is occupied either by negative silicate ions or by positive zircon ions. The form {011} can also grow with elementary growth layers with thickness d_{022} .

This enhances the prismatic habit of the theoretical growth forms. On these growth models the S form {031} could be present, if the oxygen charge $qe_o = -2|e|$ and additional strong bonds are provided by the adsorption of impurities on the surface.

- 3) Adsorption of protons, water molecules or silica complexes on the crystal surface of zircon during the growth could lead to additional hydrogen bonds parallel to $\langle 110 \rangle$. These bonds could change the S character of {110} and {001} into that of F faces.

Acknowledgements. The author acknowledges gratefully the helpful comments on the manuscript by Professor P. Hartman and the kind permission of Dr. C. Strom to use her APL computer programs CRYSTALFORM and CRYSTALDRAW.

References

- Aguiló M, Woensdregt CF (1984) Crystal morphology of ADP ($NH_4H_2PO_4$): a qualitative approach. *J Crystal Growth* 69:527-536

- Aguiló M, Woensdregt CF (1987) Theoretical growth and equilibrium forms of ADP ($\text{NH}_4\text{H}_2\text{PO}_4$). *J Crystal Growth* 83:549–559
- Caruba R (1978) Morphologie de zircons synthétiques: corrélations pétrogénétiques. *Can Mineral* 16:315–323
- Caruba R, Baumer A, Ganteaume M, Iaconni P (1985) An experimental study of hydroxyl groups and water in synthetic and natural zircons: a model of the metamict state. *Am Mineral* 70:1224–1231
- Caruba R, Baumer A, Hartman P (1988) Crystal growth of synthetic zircon round natural seeds. *J Crystal Growth* 88:297–302
- Cesbron F, Lulin J-M, Parfenoff A (1985) Un type de zircon exceptionnel: le zircon tabulaire {001} du complexe alcalin de Meponda (Mozambique); signification génétique. *Bull Minéral* 108:829–833
- Floor P (1966) Petrology of an aegirine-riebeckite gneiss-bearing part of the Hesperian Massif: The Galiñeiro and surroundings areas, Vigo, Spain. *Leidse Geol Med* 36:1–202
- Goldschmidt V (1923) *Atlas der Krystallformen*, Bd 9. Carl Winter Universitätsbuchhandlung Heidelberg
- Hartman P (1956) The morphology of zircon and potassium dihydrogen phosphate in relation to the crystal structure. *Acta Crystallogr* 9:721–727
- Hartman P (1959) Über die Gleichgewichtsformen einiger Ionenkristalle. *Neues Jahrb Mineral Monatsh*:73
- Hartman P, Bennema P (1980) The attachment energy as a habit controlling factor I. Theoretical considerations. *J Crystal Growth* 49:145–166
- Hartman P, Heijnen WMM (1983) Growth mechanisms of a crystal face for which more than one surface structure is possible. *J Crystal Growth* 63:261–264
- Hazen RM, Finger LW (1979) Crystal structure and compressibility of zircon at high pressure. *Amer Mineral* 64:196–201
- Hintze C (1915) *Handbuch der Mineralogie*, Bd I.2. Von Veit & Comp, Leipzig
- Heijnen WMM (1986) Crystal growth and morphology of calcium oxalates and carbonates. *Geol Ultraiectina* 42:11–19
- Kostov I (1973) Zircon morphology as a crystallographic indicator. *Kristall und Technik* 8:11–19
- Niggli P (1923) Kristallisation und Morphologie des rhombischen Schwefels. *Z Kristallogr* 58:490–521
- Pupin J-P, Bonin B, Tessier M, Turco G (1978) Rôle de l'eau sur les caractères morphologiques et la cristallisation du zircon dans les granitoïdes. *Bull Soc Géol France* 20:721–725
- Pupin J-P, Turco G (1981) Le zircon, minéral commun significatif des roches endogènes et exogènes. *Bull Minéral* 104:724–731
- Sillen LG (1959) *Treatises on analytical chemistry part 1, vol 1, sect B, Chap 8*. In: Kolthof IM, Elving PhJ, Sandell EB (eds) *Interscience Encyclopedia*, New York
- Söhnle O (1982) Electrolyte crystal-aqueous solution interfacial tension from crystallization data. *J Crystal Growth* 57:101–108
- Strom CS (1979) Graphical presentation of crystal habits. *J Crystal Growth* 46:185–188
- Walther JV, Orville PhM (1983) The extraction-quench technique for determination of the thermodynamic properties of solute complexes: application to quartz solubility in fluid mixtures. *Amer Mineral* 68:731–741
- Woensdregt CF (1982) Structural morphology of high sanidine (KAlSi_3O_8). *Z Kristallogr* 162:239–255
- Woensdregt CF (1992) Computation of surface energies in an electrostatic point charge model I Theory. *Phys Chem Minerals*
- Wulff G (1901) Zur Frage der Geschwindigkeit des Wachstums und der Auflösung der Krystallflächen. *Z Krist Mineral* 34:499–530